NANO · MICRO small

Supporting Information

for *Small*, DOI 10.1002/smll.202411456

A Chemically Robust Microporous Zn-MOF for C_2H_2 Separation from CO_2 and Industrially Relevant Four Component Gas Mixtures

*Bikram Pramanik, Rupam Sahoo, Rajamani Krishna and Madhab C. Das**

Supporting Information (SI)

A Chemically Robust Microporous Zn-MOF for C_2H_2 Separation from CO_2 and Industrially Relevant Four Component Gas Mixtures

Bikram Pramanik,[a] Rupam Sahoo,[a] Rajamani Krishna[b] and Madhab C. Das[a]*

[a]*Department of Chemistry, Indian Institute of Technology Kharagpur, Kharagpur 721302, WB, India.*

E-mail: mcdas@chem.iitkgp.ac.in

[b]*Van 't Hoff Institute for Molecular Sciences, University of Amsterdam, Science Park 904, 1098 XH Amsterdam, The Netherlands*

Table of Contents

	General Information	S2-S3
	Experimental section	S3-S5
Figure S1	Asymmetric unit of **IITKGP-24**	S6
Figure S2	π···π interactions in **IITKGP-24**	S6
Figure S3	TGA profile of as-synthesized and activated **IITKGP-24**	S7
Figure S4	PSD plot of **IITKGP-24**	S7
Figure S5	IAST selectivity plot at 273K and 1 bar	S7
Figure S6	Isosteric heat of adsorption plot	S8
Figure S7	Transient Breakthrough analysis of **IITKGP-24**	S8
Figure S8	Desorption curve for C_2H_2/CO_2 (50:50) mixture at 295 K	S9
Table S1-S3	Crystallographic Data	S9-S10
Table S4	DSLF parameters table of **IITKGP-24**	S10-S11
Table S5	Gas sorption comparison tables	S11-S12
	References	S12-S13

Materials and reagents:

Zinc(II) nitrate hexahydrate ($Zn(NO_3)_2 \cdot 6H_2O$, CAS #: 10196-18-6, Merck), Methyl 4-Hydroxybenzoate (Molecular Formula: $C_8H_8O_3$, CAS #: 99-76-3, TCI), 1,2-Di(4-pyridyl)ethylene (Molecular Formula: $C_{12}H_{10}N_2$, CAS #: 13362-78-2, Merck), 1,2,4,5-Tetrakis(bromomethyl)benzene (Molecular Formula: $C_{10}H_{10}Br_4$, CAS #: 15442-91-8, Thermo Scientific), Potassium carbonate (Molecular Formula: K_2CO_3, CAS #: 584-08-7, Merck), Potassium iodide (Molecular Formula: KI, CAS #: 7681-11-0, Merck), Sodium hydroxide (Molecular Formula: NaOH, CAS #: 1310-73-2, Merck), Hydrochloric acid (Molecular Formula: HCl, CAS #: 7647-01-0, Merck), Dimethylformamide (DMF, CAS #: 68-12-2, Merck), Tetrahydrofuran (THF, CAS #: 109-99-9, Merck), Methanol (CH_3OH, CAS #: 67-56-1, Merck). All reagents were obtained from commercial sources and used without further purification.

Physical Measurements:

The single-crystal XRD diffraction data were collected at 100 K on a Bruker AXS (D8 Quest System) X-ray diffractometer, equipped with a PHOTON 100 CMOS detector using graphite-monochromated *Mo-*K_α radiation (0.71073 Å). PXRD patterns were recorded using *Cu-*K_α radiation (1.5418 Å) on a Bruker D8 Advance diffractometer. Thermogravimetric analysis (TGA) was performed using a TG 209 *F3* Tarsus (Netzsch), and the sample was heated from room temperature to 800 °C at a rate of 5 °C min^{-1} under N_2 atmosphere. Gas sorption experiments were tested on a Micromeritics *3-Flex* Surface Characterization Analyzer at different temperatures (273 K and 295 K). A chiller was used for the gas sorption measurements. BET surface area analysis was performed at 195 K CO_2 sorption as no appreciable surface area was found at 77 K N_2 sorption. All the guest molecules in the framework were removed by degassing the sample at 353 K for 10 h until the outgassing rate was 5 μmHg/min prior to measurements.

Crystallographic Data and Structure Refinements:

Good quality single crystal of **IITKGP-24** was sorted out with the help of a polarizing microscope and immersed in paratone oil, which was then mounted on the tip of glass fiber and cemented using epoxy resin. The single-crystal XRD diffraction data were collected at 100 K on a Bruker AXS (D8 Quest System) X-ray diffractometer, equipped with a PHOTON 100 CMOS detector using graphite-monochromated *Mo-*K_α radiation (0.71073 Å). The linear absorption coefficients, scattering factors for the atoms, and the anomalous dispersion corrections were taken from International Tables for X-ray Crystallography. Bruker Apex III software was used for data collection, unit cell measurements, absorption corrections, scaling,

and integration.[1,2] The data were reduced and an empirical absorption correction was applied with the help of SAINTPLUS software and SADABS programs using XPREP, respectively.[3,4] The structures were solved by the direct method using SHELXL-2014 in the WinGx programs. The WinGx package of programs was used to carry out the full-matrix least-squares refinement against the function $|F^2|$.[5,6] Attempts to identify the highly disordered solvent molecules for **IITKGP-24** was failed. Instead, a new set of F^2 (hkl) values with the contribution from the solvent molecules were obtained by the *SQUEEZE* procedure implemented in *PLATON*.[7] For all the cases, non-hydrogen atoms were refined anisotropically. All hydrogen atoms were geometrically fixed using the riding atom model and assigned fixed isotropic displacement parameters. The "ACTA" command was used to generate the Crystallographic Information File (CIF). The structural details of the compound are presented in **Table S1**. **CCDC: 2404969** contains the crystallographic data for **IITKGP-24**. These data are available from the Cambridge Crystallographic Data Center (CCDC) *via* www.ccdc.cam.ac.uk/data_request/cif.

Synthesis of 1,2,4,5-tetrakis[(4-carboxy)phenoxymethyl]benzene (H_4L):

1,2,4,5-tetrakis[(4-carboxy)phenoxymethyl]benzene (H_4L) was synthesized according to the previous literature report (**Scheme S1**).[8] A mixture of methyl 4-hydroxybenzoate (9.13 g, 60 mmol), along with catalytic amount of KI (74 mg, 4.4 mmol), and K_2CO_3 (36 g, 260 mmol) was charged in an 500 ml round bottom flask and dissolved in 250 ml DMF. Then the resulting solution was heated to 100 °C for 1 hour. After that, 1,2,4,5-Tetrakis(bromomethyl)benzene (3.6 g, 8 mmol) was dissolved in DMF (20 ml), added dropwise to the mixture, followed by heating at 100 °C for additional 4 hours and then cooled to room temperature. Approximately 800 ml of water was added to the solution to produce a precipitate, which was filtered at suction, washed thoroughly with water, and dried on air to give 5.8 g (99 %) of the white solid. After that, this synthesized tetramethyl ester (5.8 g, 7.9 mmol) was added to a 500 ml round bottom flask containing tetrahydrofuran (150 ml) and methanol (50 mL). An aq. NaOH solution (4.9 g, 120 mmol in 200 ml H_2O) was added to this mixture and then heated at 60 °C for 12 h. The solution was concentrated, diluted with water to dissolve the salts, then acidified to pH = 1 using 6 N HCl. The precipitate was separated by filtration at suction, washed thoroughly with water, and dried on air to yield 5.0 g (89 %) of white solid. ^{1}H NMR (400 MHz, DMSO-d_6): δ = 12.6 (bs, 4H), 7.88 (d, J=8.9, 8H), 7.74 (s, 2H), 7.10 (d, J=8.9, 8H), 5.33 (s, 8H).

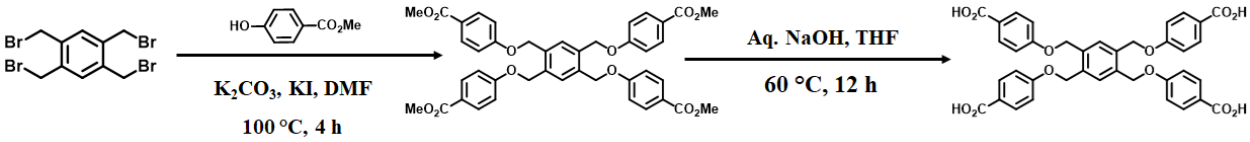

Scheme S1: Schematic representation of H_4L ligand synthesis.

Synthesis of IITKGP-24:

A mixture of $Zn(NO_3)_2 \cdot 6H_2O$ (0.05 mmol, 0.015 g), H_4L (0.0125 mmol, 0.008 g), and 1,2-Di(4-pyridyl)ethylene (0.05 mmol, 0.009 g) was taken in a 15 ml glass vial containing 5 ml of DMF solvent. After that 100 µl of acetic acid was added to the reaction mixture. Then the resulting mixture was allowed to stir for 30 minutes and transferred to the hydrothermal oven at 85 °C for 3 days, followed by slow cooling at the rate of 5 °C/h. Colourless pellet-shaped good-quality crystals were observed after cooling, suitable for single crystal X-ray diffraction. The crystals were collected by filtration, rinsed three times with DMF, and stored in fresh DMF solvent, giving a yield of 65% based on $Zn(NO_3)_2 \cdot 6H_2O$.

Fitting of unary isotherm data:

The unary isotherms for C_2H_2, C_2H_4, C_2H_6 and CO_2 measured at two different temperatures 273 K, and 295 K in **IITKGP-24** were fitted with excellent accuracy using either the dual-site Langmuir model, where we distinguish two distinct adsorption sites A and B:

$$q = \frac{q_{sat,A} b_A p}{1 + b_A p} + \frac{q_{sat,B} b_B p}{1 + b_B p} \tag{S1}$$

In eq (S1), the Langmuir parameters b_A, b_B are both temperature dependent

$$b_A = b_{A0} \exp\left(\frac{E_A}{RT}\right); \quad b_b = b_{B0} \exp\left(\frac{E_B}{RT}\right) \tag{S2}$$

In eq (S2), E_A, E_B are the energy parameters associated with sites A, and B, respectively.

The unary isotherm fit parameters are provided in **Table S4**.

Isosteric heat of adsorption:

The isosteric heat of adsorption, Q_{st}, is defined as

$$Q_{st} = -RT^2 \left(\frac{\partial \ln p}{\partial T}\right)_q \tag{S3}$$

where, the derivative in the right member of eq (S3) is determined at constant adsorbate loading, q. the derivative was determined by analytic differentiation of the combination of eq (S1), eq (S2), and eq (S3).

IAST calculations of adsorption selectivities:

For separation of binary mixtures of components 1 and 2, the adsorption selectivity, S_{ads}, is defined by

$$S_{ads} = \frac{q_1/q_2}{y_{10}/y_{20}} \qquad \text{(S4)}$$

In eq (S4), y_{10}, y_{20} are the mole fractions of the bulk gas phase mixture.

The molar loadings q_1, q_2 of the two components are determined using the Ideal Adsorbed Solution Theory (IAST) of Myers and Prausnitz[9] using the unary isotherm fits as data inputs. IAST calculations were carried out for C_2H_2/CO_2 (50:50) at 273 K and 295 K.

Transient breakthrough simulations:

Transient breakthrough simulations for C_2H_2/CO_2 (50:50) and $C_2H_2/C_2H_4/C_2H_6/CO_2$ (25:25:25:25) mixtures were carried out for the adsorption cycle in a fixed bed operating at a total pressure of 100 kPa, and temperatures of 273 K and 295 K. The methodology used for the transient breakthrough simulations are the same as described in earlier publications.[10-15] In these simulations, intra-crystalline diffusion influences are ignored. For these simulations we specify: length of packed bed, L = 0.3 m; cross-sectional area, A = 1 m^2; volumetric flow rate at the entrance to the bed, $Q_0 = 40$ L s^{-1}; voidage of the packed bed, ε = 0.4. The volume of MOF used in the simulations is $V_{ads} = LA(1-\varepsilon)$. It is important to note that the volume of adsorbent, V_{ads}, includes the pore volume of the adsorbent material. If ρ is the framework density, the mass of the adsorbent in the bed is $m_{ads} = (1-\varepsilon)\times(L \text{ m})\times(A \text{ m}^2)\times(\rho \text{ kg m}^{-3})$ kg.

Purified C_2H_2 can be recovered in the desorption cycle of PSA operations. Simulations of the desorption phase were also undertaken using deep vacuum. The desorption data are shown in **Figure S8**.

For presentation of the results of the breakthrough simulations, the dimensionless concentrations at the exit, c_i/c_{i0} are plotted as a function of the parameters $\frac{(Q_0 = \text{flow rate L s}^{-1})\times(\text{time in s})}{(\text{kg MOF packed in tube})} = \frac{Q_0 t}{m_{ads}} = \text{L kg}^{-1}$. It is also to be noted that we use the modified time parameter $\frac{Q_0 t}{m_{ads}}$ instead of the dimensionless breakthrough time, τ, used in earlier works of Cui *et al* and Das *et al*.[16,17]

Notation:

b: Langmuir constant, Pa^{-1}

c_i: molar concentration of species i, mol m^{-3}

c_{i0}: molar concentration of species i in fluid mixture at inlet, mol m^{-3}

E: energy parameter, J mol^{-1}

L: length of packed bed adsorber, m

m_{ads} : mass of adsorbent packed in fixed bed, kg

Q: component molar loading of species i, mol kg^{-1}

q_{sat}: saturation loading, mol kg^{-1}

Q_0 : volumetric flow rate of gas mixture entering fixed bed, m^3 s^{-1}

Q_{st} : isosteric heat of adsorption, J mol^{-1}

T : absolute temperature, K

Greek alphabet:

ε : voidage of packed bed, dimensionless

ρ : framework density, kg m^{-3}

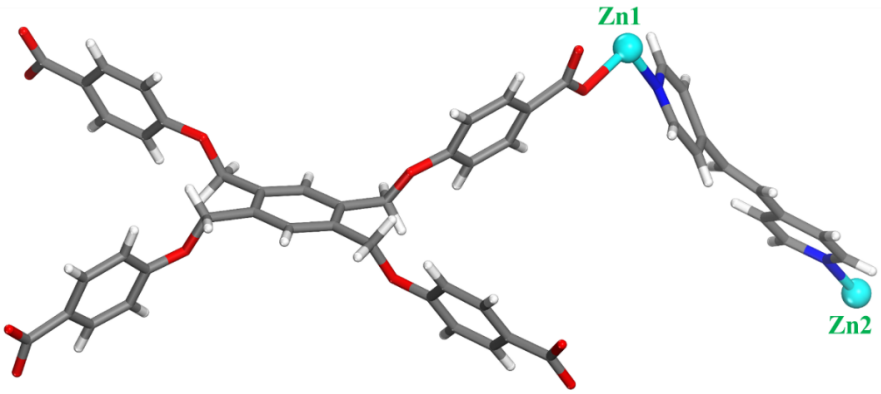

Figure S1: Asymmetric unit of **IITKGP-24**. (Color codes: Zn, Cyan; O, red; N, blue; C, gray; H, white).

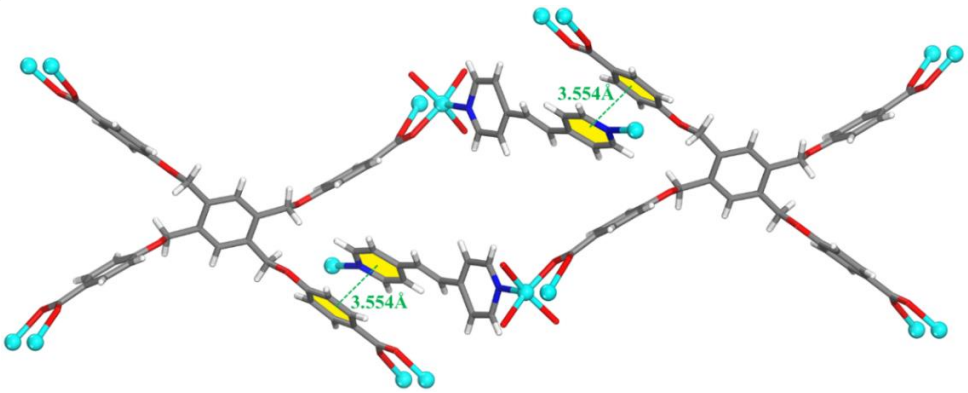

Figure S2: Representation of π···π stacking interactions in **IITKGP-24**. (Color codes: Zn, Cyan; O, red; N, blue; C, gray; H, white).

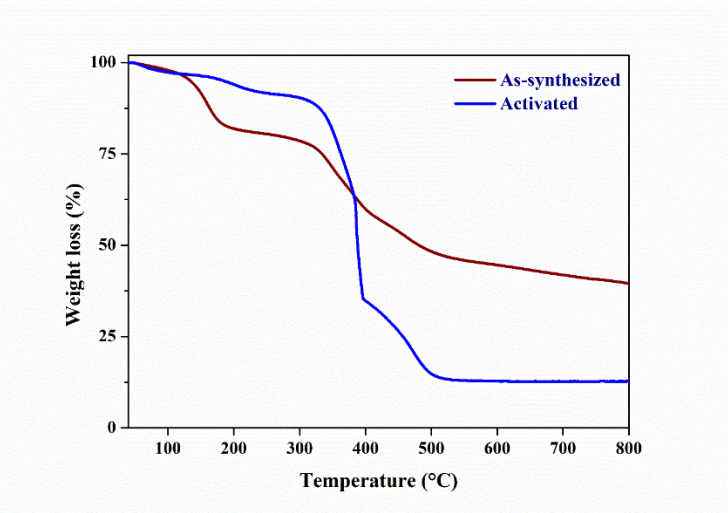

Figure S3: Thermogravimetric analysis (TGA) profile of as-synthesized **IITKGP-24** and activated sample **IITKGP-24a**. Activated MOF, **IITKGP-24a** shows some weight loss before degradation. It may be noted that the gradual weight loss of the activated sample could be attributed to the removal of surface adsorbed water molecules during the quick transfer process of activated sample from an inert sealed tube to the TGA crucible.

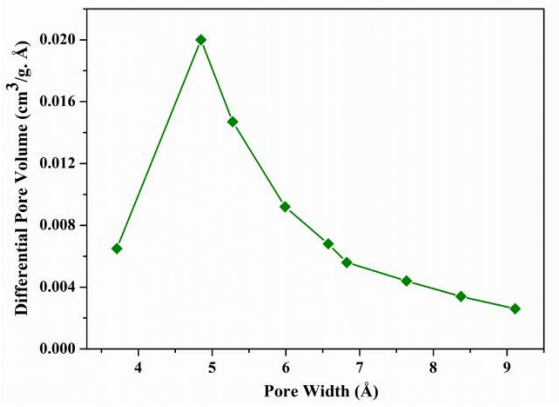

Figure S4: Pore size distribution (PSD) plot derived from the 195 K CO_2 isotherm by applying Horvath-Kawazoe analysis indicating average pore width of 4.8 Å, well-agreement with the crystallographic pore space analysis.

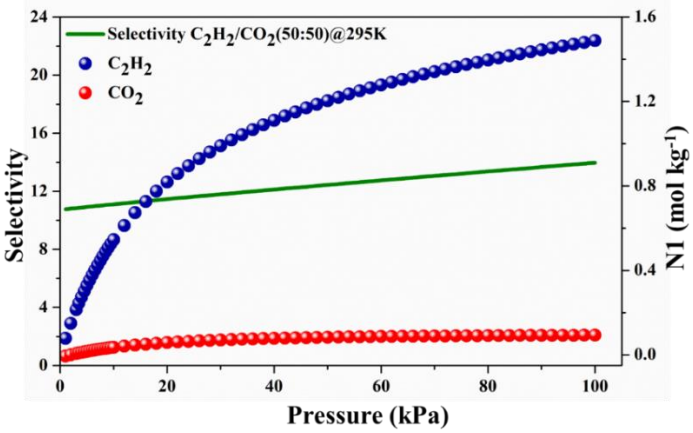

Figure S5: IAST selectivity of (50:50) C_2H_2/CO_2 mixture at 273 K and 1 bar.

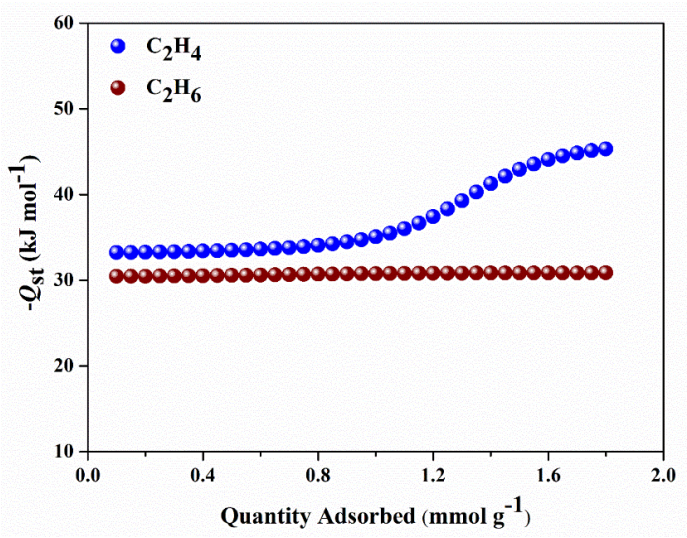

Figure S6: Isosteric heat of adsorption (Q_{st}) for C_2H_4 and C_2H_6 gases.

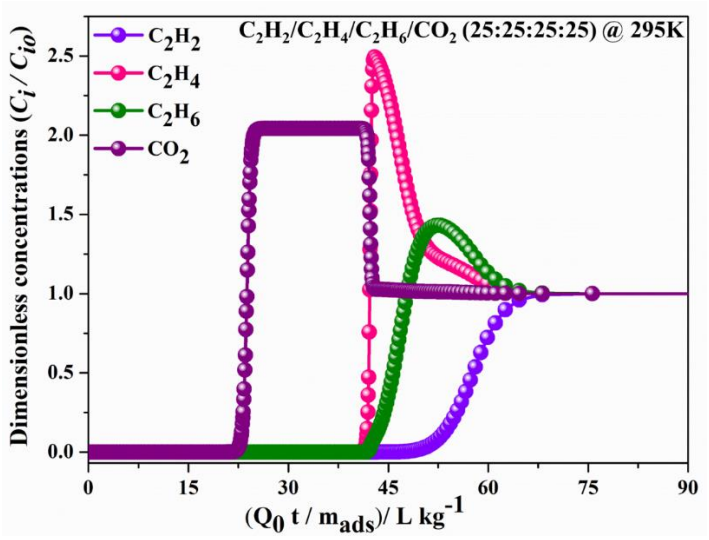

Figure S7: Transient breakthrough simulations of **IITKGP-24** for separation of $C_2H_2/C_2H_4/C_2H_6/CO_2$ (25:25:25:25) mixture in a fixed bed operating at 100 kPa, and 295 K. The x-axis represents (Q_0t/m_{ads}) as modified time parameter.

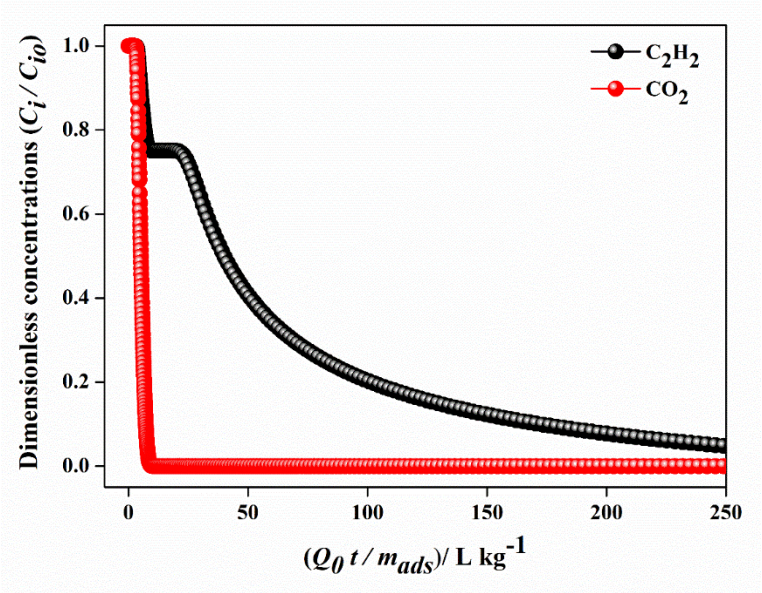

Figure S8: The desorption curve of **IITKGP-24** for the C_2H_2/CO_2 (50:50) mixture under deep vacuum at 295 K. The x-axis represents (Q_0t/m_{ads}) as modified time parameter.

Table S1: Crystal data and structure refinements for **IITKGP-24**.

Empirical formula	$C_{50}\ H_{36}\ N_2\ O_{12}\ Zn_2$
Formula weight	987.59
Temperature (K)	100
Radiation	*Mo* (K_α)
Wavelength (λ) [Å]	0.71073
Crystal system	Triclinic
Space group	$P\bar{1}$
a [Å]	12.986(11)
b [Å]	16.112(14)
c [Å]	19.264(19)
α [°]	67.85(3)
β [°]	88.87(3)
γ [°]	85.05(3)
Volume [Å^3]	3719(6)
Z	2
Density (calculated)[Mg m^{-3}]	0.882
Absorption coefficient [mm^{-1}]	0.685
F (000)	1012
Refl. used [$I > 2\sigma(I)$]	16375
Independent reflections	7863
R_{int}	0.085
Refinement method	full-matrix least squares on F^2
GOF	0.861

Final *R* indices[$I>2\sigma(I)$]	R_1= 0.0698, wR_2 = 0.1803
R indices (all data)	R_1= 0.1245, wR_2 = 0.1999
CCDC	**2404969**

Table S2: Selected Bond Distances (Å) and Bond Angles (º) in **IITKGP-24**.

Selected bond lengths [Å]

Zn1–O1	2.020(4)	Zn2–N2	2.042(4)
Zn1–N1	2.031(5)	Zn2–O6#4	2.066(3)
Zn1–O5#1	2.043(4)	Zn2–O11#5	2.054(3)
Zn1–O12#2	2.033(3)	Zn2–O2#6	2.044(4)
Zn1–O8#3	2.069(4)	Zn2–O9#7	2.031(3)

Selected bond angles [º]

O1–Zn1–N1	101.82	O6#4–Zn2–N2	96.36(14)
O1–Zn1–O5#1	87.35(12)	O11#5–Zn2–N2	109.04(14)
O1–Zn1–O12#2	162.59(14)	O2#6–Zn2–N2	94.47(15)
O1–Zn1–O8#3	90.79(12)	O9#7–Zn2–N2	102.27(14)
O5#1–Zn1–N1	106.23	O6#4–Zn2–O11#5	89.46(12)
O12#2–Zn1–N1	95.55	O2#6–Zn2–O6#4	86.22(12)
O8#3–Zn1–N1	95.52	O6#4–Zn2–O9#7	161.26(13)
O5#1–Zn1–O12#2	88.91(12)	O2#6–Zn2–O11#5	156.43(14)
O5#1–Zn1–O8#3	158.09(14)	O9#7–Zn2–O11#5	86.36(12)
O8#3–Zn1–O12#2	86.37(12)	O2#6–Zn2–O9#7	90.34(12)

Symmetry transformations used to generate equivalent atoms: #1 = -1+x, y, z; #2 = -1+x, y, 1+z; #3 = x, y, 1+z; #4 = -1+x, 1+y, z; #5 = -1+x, 1+y, 1+z; #6 = x, 1+y, z; #7 = x, 1+y, 1+z;

Table S3: Non-covalent hydrogen-bonding interactions in **IITKGP-24**.

D–H···A	**d(H···A)(Å)**	**D(D···A)(Å)**	**∠DHA(º)**
C8–H8A···O4	2.49	3.023(7)	114
C15–H15A···O3	2.57	3.055(7)	110
C23–H23B···O7	2.52	3.112(7)	118
C28–H28···O12	2.43	2.759(7)	100
C31–H31B···O10	2.53	3.111(8)	117
C36–H36···O3	2.58	3.456(7)	153
C48–H48···O6	2.46	3.082(7)	123

Table S4: Dual-site Langmuir fits for guest molecules in **IITKGP-24**.

	Site A			Site B		
	$q_{A,sat}$ / mol/kg	b_{A0} / Pa^{-1}	E_A / kJ mol^{-1}	$q_{B,sat}$ / mol/kg	b_{B0} / Pa^{-1}	E_B / kJ mol^{-1}
C_2H_2	1.6	5.989E-10	29.5	2.2	6.625E-10	20.3

C_2H_4	0.6	1.969E-14	46.6	1.3	1.476E-10	33
C_2H_6	1.2	6.614E-11	30.9	0.7	1.197E-09	30.4
CO_2	0.36	6.541E-24	16	1.5	1.576E-10	27.2

Table S5: Comparison of adsorptive separation properties of **IITKGP-24** with the reported various MOFs in literature, including C_2H_2, and CO_2 uptake capacity, C_2H_2/CO_2 selectivity, heat of adsorption data, adsorption capacity of C_2H_2 (Operational conditions: 298 K and 1.0 bar). Other than **IITKGP-24**, the productivity was calculated from experimentally dynamic breakthrough separations.

Sl. No.	MOFs/CPs	C_2H_2 Uptake (cc g^{-1})	CO_2 Uptake (cc g^{-1})	IAST selectivity C_2H_2/CO_2 (50:50)	Q_{st} of C_2H_2 (kJ mol^{-1})	Productivity of C_2H_2 (mmol g^{-1})	Reference
1	**IITKGP-24**	**43.6**	**15.3**	**13.9**	**29.2**	**1.38**	**This Work**
2	PCN-200	40	32	6.4	57	–	*Sep. Purif. Technol.* **2023**, *324*, 124557
3	ZNU-11	45.5	22.5	8.2	36.1	1.41	*Sep. Purif. Technol.* **2024**, *332*, 125777
4	ZNU-4	85.1	44	9	50.3	–	*Chem. Eng. J.* **2022**, *450*, 138034
5	UPC-80	77.2	39.2	6.34	20.84	1.29	*Chem. Eng. J.* **2023**, *453*, 139713
6	SIFSIX-DPA-Cu-i	75.59	50.17	9.34	46.53	–	*Chem. Eng. J.* **2023**, *477*, 147001
7	JCM-1	75	38	13.7	36.9	2.2	*Angew. Chem. Int. Ed.* **2018**, *57*, 7869 –7873
8	CPL-1-NH_2	41.2	4.7	119	50	–	*Angew. Chem. Int. Ed.* **2021**, *60*, 4570 –4574
9	sql-SIFSIX-bpe-Zn	40	40	8.4	67.5	–	*Angew. Chem. Int. Ed.* **2021**, *60*, 20383 – 20390
10	SNNU-98-Mn	111.56	67.82	22.7	60.2	4.9	*Angew. Chem. Int. Ed.* **2023**, *62*, e202217839
11	SNNU-98-Co	72.36	42.26	14.4	53.5	1.9	
12	SNNU-98-Ni	67.79	46.79	3.3	39.3	2.8	
13	SNNU-98-Zn	70.47	38.01	17.4	41.3	2.2	
14	SNNU-37(Fe)	108.9	47.7	9.9	34.4	–	*Inorg. Chem.* **2021**, *60*, 18473−18482
15	SNNU-37(Sc)	78.1	34	2.7	26.5	–	
16	UTSA-220	76.1	75.7	4.4	29	–	*ACS Sustainable Chem. Eng.* **2019**, *7*, 4897−4902
17	FJU-36	52.2	35.5	2.2	32.9	–	*Inorg. Chem.* **2018**, *57*, 12961−12968
18	MUF-17	67.4	56.2	6.0	49.5	2.06	*Chem. Mater.* **2019**, *31*, 4919−4926
19	CAU-10-H	89.8	58.7	4.6	25.2	–	

20	CAU-10-CH_3	78.2	31.6	4.0	25	–	*Chem Bio Eng.* **2024**, *1*, 245−251
21	[Ni_2(BTEC)(bipy)$_3$]	76.8	13.0	33.5	19.8	2.08	*Sep. Purif. Technol.* **2021**, *256* 117749
22	NKMOF-1-Ni	61	51.1	20	60.3	–	*Angew. Chem. Int. Ed.* **2018**, *57*, 10971 – 10975
23	ZJU-280	106.2	70.6	18.1	50.6	4.1	*J. Mater. Chem. A.* **2021**, *9*, 9248–9255
24	UTSA-74	107	71	9.0	31	–	*J. Am. Chem. Soc.* **2016**, *138*, 5678−5684
25	IITKGP-25	58.1	42.8	3.93	26.6	–	*Inorg. Chem.* **2022**, *61*, 18293−18302
26	CTGU-39	65.5	44.5	8.4	26.8	–	*Sep. Purif. Technol.* **2024**, *344* 127286
27	CTGU-40	74.1	49.5	3.3	27.8	–	
28	JNU-5-Me	105.3	5.6	18.5	37.4	–	*Chem Bio Eng.* **2024**, *1*, 150−156
29	bpy-NH2- CuZrF6	138.9	84.8	6.6	37.1	2.3	*Chem. Eng. J.* **2024**, *498*, 155574

References:

1. G. M. Sheldrick, Siemens Area Correction Absorption Correction Program; University of Göttingen: Göttingen, Germany, **1994**.
2. L. J. Farrugia, WinGx suite for small-molecule single crystal crystallography. *J. Appl. Crystallogr.* **1999**, *32*, 837.
3. SAINT+, 6.02ed, Bruker AXS, Madison, WI, **1999**,
4. XPREP, 5.1 ed. Siemens Industrial Automation Inc., Madison, WI, **1995**,
5. G. M. Sheldrick, SHELXL-97 Program for Crystal Structure Solution and Refinement; University of Göttingen: Göttingen, Germany, **1997**.
6. G. M. Sheldrick, Crystal Structure Refinement with SHELXL. *Acta Cryst C* **2015**, *71*, 3–8.
7. Platon Program: Spek, A. L. *Acta Crystallogr. Sect. A*, **1990**, *46*, 194.
8. R. Sahoo, B. Pramanik, S. Mondal, M. C. Das, A Highly Chemically Robust 3D Interpenetrated MOF Heterogeneous Catalyst for the Synthesis of Hantzsch 1,4-Dihydropyridines and Drug Molecules. *Small* **2024**, *20*, 2309281.
9. R. Krishna, The Maxwell-Stefan Description of Mixture Diffusion in Nanoporous Crystalline Materials. *Microporous Mesoporous Mater.* **2014**, *185*, 30-50. https://doi.org/10.1016/j.micromeso.2013.10.026.
10. R. Krishna, Methodologies for Evaluation of Metal-Organic Frameworks in Separation Applications. *RSC Adv.* **2015**, *5*, 52269-52295. https://doi.org/10.1039/C5RA07830J.
11. R. Krishna, Screening Metal-Organic Frameworks for Mixture Separations in Fixed-Bed Adsorbers using a Combined Selectivity/Capacity Metric. *RSC Adv.* **2017**, *7*, 35724-35737. https://doi.org/10.1039/C7RA07363A.
12. R. Krishna, Methodologies for Screening and Selection of Crystalline Microporous Materials in Mixture Separations. *Sep. Purif. Technol.* **2018**, *194*, 281-300. https://doi.org/10.1016/j.seppur.2017.11.056.
13. R. Krishna, Metrics for Evaluation and Screening of Metal-Organic Frameworks for Applications in Mixture Separations. *ACS Omega* **2020**, *5*, 16987−17004. https://doi.org/10.1021/acsomega.0c02218.

14. R. Krishna, Synergistic and Antisynergistic Intracrystalline Diffusional Influences on Mixture Separations in Fixed Bed Adsorbers. *Precision Chemistry* **2023**, *1*, 83-93. https://doi.org/10.1021/prechem.2c00003.
15. R. Krishna, Fundamental Insights into Intra-Crystalline Diffusional Influences on Mixture Separations in Fixed Bed Adsorbers. *Chem Bio Eng*. **2024**, *1*, 53-66. https://doi.org/10.1021/cbe.3c00057.
16. X. Cui, K. Chen, H. Xing, Q. Yang, R. Krishna, Z. Bao, H. Wu, W. Zhou, X. Dong, Y. Han, B. Li, Q. Ren, M.J. Zaworotko, B. Chen. Pore Chemistry and Size Control in Hybrid Porous Materials for Acetylene Capture from Ethylene, *Science* **2016**, *353*, 141-144. https://doi.org/10.1126/science.aaf2458.
17. M. C. Das, Q. Guo, Y. He, J. Kim, C. G. Zhao, K. Hong, S. Xiang, Z. Zhang, K.M. Thomas, R. Krishna, B. Chen, Interplay of Metalloligand and Organic Ligand to Tune Micropores within Isostructural Mixed-Metal Organic Frameworks (M'MOFs) for Their Highly Selective Separation of Chiral and Achiral Small Molecules. *J. Am. Chem. Soc*. **2012**, *134*, 8703-8710. https://doi.org/10.1021/ja302380x.